Influence of visible light LEDs modulation techniques on photocatalytic degradation of ceftriaxone in a flat plate reactor

Nicola Morante [a], Olimpia Tammaro [b], Luisa Albarano [c], Luca De Guglielmo [g], Nunzio Oliva [g], Olga Sacco [e], Antonietta Mancuso [a], Micaela Castellino [b], Diana Sannino [a], Nicola Femia [d], Giusy Lofrano [f], Giovanni Libralato [c], Serena Esposito [b,*], Vincenzo Vaiano [a,*]

[a] *Department of Industrial Engineering, University of Salerno, Via Giovanni Paolo II 132, 84084 Fisciano, SA, Italy*
[b] *Department of Applied Science and Technology and INSTM Unit of Torino – Politecnico, Politecnico di Torino, Corso Duca degli Abruzzi 24, 10129 Torino, Italy*
[c] *Department of Biology, University of Naples Federico II, Monte Sant'Angelo University Complex – Building 7, Via Vicinale Cupa Cintia 26, 80126, Naples, Italy*
[d] *Department of Information, and Electrical Engineering and Applied Mathematics, University of Salerno, Via Giovanni Paolo II 132, 84084 Fisciano, SA, Italy*
[e] *Department of Chemistry and Biology "A. Zambelli", University of Salerno, Via Giovanni Paolo II, 132, 84084 Fisciano, SA, Italy*
[f] *Department of Movement, Human and Health Sciences, University of Rome Foro Italico, Piazza Lauro De Bosis, 15, 00135 Roma, Italy*
[g] *EXELING SRL, Contrada S. Tommaso 18/F, 83100 Avellino, Italy*

ABSTRACT

In this paper, the effect of light modulation on photocatalytic ceftriaxone (CEF) degradation in aqueous solution was investigated. The experimental set-up consisted of a fixed bed photocatalytic reactor with a flat plate geometry and visible LEDs for irradiation. Fe-N-codoped TiO$_2$ photocatalyst was immobilized on a polystyrene plate (PS) by solvent casting method to achieve a structured photocatalyst (Fe-N-TiO$_2$/PS), which was loaded in the photoreactor. Raman and UV–Vis diffuse reflectance spectroscopy confirmed the presence of Fe-N-TiO$_2$ on the PS surface and its uniform distribution on the polymer support. Various LEDs dimming techniques were tested with fixed and variable duty-cycle values. In particular, the following modulations were used: fixed duty-cycle (FD), sinusoidal variable duty-cycle (S-VD), triangular variable duty-cycle (T-VD), square wave variable duty-cycle (SW-VD), saw-tooth variable duty-cycle (ST-VD), pulse variable duty-cycle (P-VD), and pseudo-sinusoidal variable duty-cycle (PS-VD). The optimal light modulation was the S-VD, with an average fed current between 25 and 75 mA and a period of 30 s. Indeed, by using S-VD modulation, the highest value of the apparent CEF degradation kinetic constant (resulting 0.0082 min^{-1}) and the highest total organic carbon (TOC) removal (70 %) were achieved. By comparing the electric energy consumption (E$_{E/O}$) with S-VD modulation used in this work with those found in other literature studies dealing with the photocatalytic ceftriaxone degradation, a significant decrease of E$_{E/O}$ was evidenced. Moreover, toxicity test showed that the photocatalytic treatment allowed to significantly reduce the toxicity of CEF solution when compared to untreated effluent.

1. Introduction

Thanks to advances in science and technology, the research-based pharmaceutical industry has shown high growth rates significantly contributing with even new pharmaceuticals to improvements in patient well-being [1]. Pharmaceutical consumption has been increasing worldwide in the last decades determining a continuous release of these compounds or their metabolites into the environment. Among the various pharmaceutical products, antibiotics are frequently used for the treatment of human and veterinary bacterial infections, and for this

reason, there was an increase in the concentration of these pollutants and their metabolites in wastewater [2]. Antibiotics are classified as emerging contaminants, and despite the low concentrations, they are persistent and potentially toxic to microorganisms due to their complicated molecular structure, threatening the environment and human health. It has been reported that they can act on the physical or cerebral characteristics of the fish fauna, negatively influencing marine biodiversity [3]. Depending on the source from which they are released, antibiotics are detected in waters in a wide range of concentrations, which can vary from a few ppb up to ppm [4–6]. Among the different

antibiotics, ceftriaxone (CEF) is widely used for human treatment and animal husbandry due to its broad-spectrum antimicrobial activity, which results in the release of residues into wastewater, thereby causing ecological, environmental, and health issues. Furthermore, CEF is persistent and hard to degrade by conventional treatment methods, and it may cause bacterial drug resistance [7–9]. For this reason, the treatment of wastewater containing CEF with appropriate, cost-effective, and high-efficiency methods is a challenging issue. Advanced oxidation processes (AOPs), which are based on the generation of reactive oxygen species (ROS) within the treatment system, represent a promising alternative for the treatment of antibiotics wastewater [10–14].

Among different AOPs, the visible-light driven photocatalysis carried out by irradiating a suitably structured photocatalyst (realized through the immobilization of a photocatalyst on the surface of macroscopic support) with modulated light using the dimming technique is one of the new and cost-effective methods for the removal of recalcitrant contaminants from wastewater [15–18]. The use of a structured photocatalyst active in the visible allows to overcome the limits of the slurry reactors, and to exploit sunlight or visible light for the decontamination of the wastewater [19]. Furthermore, the use of modulated irradiation plays a crucial role in increasing the pollutant degradation rate, enabling the photocatalytic process to be intensified. Indeed, alternating light and dark periods give rise to improved photonic efficiency, reducing the recombination rate of the photogenerated pairs, and increasing the ROS concentration within the reaction system [20]. In our previous works [15–18], it was shown that the irradiation with the modulation of visible LEDs dimming duty cycle remarkably enhanced the photocatalytic performances towards the degradation of probe organic molecules (organic dyes, urea and terephthalic acid). Based on the promising obtained results, we have chosen to test the influence of visible light modulation techniques in the photocatalytic degradation and mineralization of a pollutant of emerging concern.

To our best knowledge, no paper has been found in the literature devoted to the use of visible light LEDs modulation techniques in a photocatalytic system to degrade CEF and on the evaluation of toxicological results on the effluents coming from photocatalytic systems based on light modulation techniques. For this reason, this paper aims to study the influence of controlled modulation of visible light emitted by LEDs on the performances of a flat plate photocatalytic reactor for CEF degradation in the presence of Fe-N-codoped TiO$_2$ photocatalyst (Fe-N-TiO$_2$) immobilized on a polystyrene plate (PS). Moreover, toxicity tests were carried out to evaluate larval and adult-related effects of treated effluents on *Artemia franciscana*.

2. Materials and methods

2.1. Chemicals

Titanium tetraisopropoxide (TTIP, Sigma Aldrich, 97 %), urea (CH$_4$N$_2$O, Sigma Aldrich, 99.5 %), iron(II) acetylacetonate (Sigma Aldrich, 99.9 %), ceftriaxone disodium salt hemiheptahydrate (Sigma Aldrich, ≥99.%), acetone (Sigma Aldrich, ≥99.5 %), polystyrene plate (Wessex Pictures) and distilled water were purchased. The molecular structure of CEF is shown in Fig. S1.

2.2. Preparation of the structured photocatalyst (Fe-N-TiO$_2$/PS)

Fe-N-TiO$_2$ photocatalyst used for this experimentation were chosen based on the optimization studies performed in our previous works [21,22]. Fe-N-TiO$_2$ in powder form was prepared via sol–gel method, using urea as nitrogen precursor, iron (II) acetylacetonate as iron precursor, and titanium tetraisopropoxide as TiO$_2$ precursor. First, 1.2 g of urea was added to 50 mL of distilled water and the resultant solution was stirred for 5 min (solution A). For the next step, 25 mg of iron(II) acetylacetonate was dissolved in 12.5 mL of TTIP (solution B). Then, solution B was added dropwise into solution A. The mixture was

maintained at room temperature under continuous stirring. The obtained suspension was centrifuged and washed with distilled water three times, and finally calcined at 450 °C for 30 min in static air, using a muffle furnace.

The support used for the immobilization of the photocatalyst was a polystyrene plate (PS) (size: 31 × 11 × 0.2 cm). The structured photocatalyst, named Fe-N-TiO$_2$/PS, was prepared by a solvent-assisted method, following the procedure reported in our previous works [18,23].

Initially, 1.68 g of Fe-N-TiO$_2$ photocatalyst was dispersed in 40 mL of acetone. The resulting suspension was subjected to sonication in an ultrasonic bath (CEIA CP104 standard ultrasonic cleaner) for 5 min at a power of 95 %, and a temperature of 20 °C. Subsequently, the suspension was spread onto the surface of the support using a Gilson micropipette at room temperature. Thanks to the action induced by acetone, which acts as a solvent for the PS, Fe-N-TiO$_2$ particles adhered to the external surface of the PS plate. Finally, the Fe-N-TiO$_2$/PS plate was dried at room temperature for 24 h. The excess of Fe-N-TiO$_2$ particles not immobilized on the PS plate were removed by means of several cycles in an ultrasonic bath (CEIA-CP104) until to reach a stable loading of the structured photocatalyst. The amount of photocatalyst deposited on the PS plate was measured by an analytical balance (Ohaus Mettler Toledo, 0.1 mg resolution), and the final loading of Fe-N-TiO$_2$ was found to be about 5.7 wt%.

2.3. Photocatalyst characterization

X-ray Photoelectron Spectroscopy (XPS) has been conducted on bare TiO$_2$ powder (prepared with the same method used for the synthesis of doped catalyst but without using urea and iron(II) acetylacetonate) and on the Fe-N-TiO$_2$ one, by means of a PHI 5000 Versaprobe spectrometer (Physical Electronics, Chanhassen, MN, USA), equipped with a monochromated K-alpha source (1486.6 eV), with a double charge compensation system, made up by an electron beam and an ion (Ar$^+$) beam. Survey and High Resolution (HR) spectra have been acquired for each sample, to infer chemical composition and elements oxidation states. CasaXPS 2.3.18 dedicated software has been applied to perform the deconvolution procedure on raw data. C1s peak at 284.8 eV has been used as a reference for the Binding Energy scale axis.

The photoluminescence (PL) spectra were recorded at room temperature using a fluorescence spectrometer LS 55PerkinElmer with an Xe lamp as the excitation source. The samples were excited using light of a wavelength of 362 nm.

Raman spectra of the structured photocatalyst and PS plate were obtained at ambient temperature in the range of 100–1700 cm^{-1} Raman shift using a Dispersive Micro Raman (Invia, Renishaw) equipped with a 514 nm laser. The UV–vis reflectance spectra (UV–vis DRS) were performed by a PerkinElmer spectrophotometer Lambda 35 equipped with an RSA–PE–20 reflectance spectroscopy accessory (Labsphere Inc., North Sutton, NH).

2.4. Experimental set-ups setup used for photocatalytic tests

Initially, photocatalytic activity tests were conducted inside a slurry photocatalytic reactor (SPR). Subsequently, the influence of light modulation on the photocatalytic activity of Fe-N-TiO$_2$/PS was analyzed using a recirculating flate plate photocatalytic reactor (RPR).

2.4.1. SPR

The SPR was a Pyrex cylindrical tank (I.D. = 10 cm; height = 6.0 cm) equipped with a magnetic stirrer and an air distributor device positioned inside the reactor (Q_{air} = 150 Ncm^3 min^{-1}). The magnetic stirrer and the distributor device assured a homogeneous presence of oxygen in the solution to be treated and avoided the sedimentation of the photocatalyst nanopowders. A cooling fan was positioned near the photocatalytic system to avoid the increase of reaction temperature at values

higher than 35 °C. The solution volume was 100 mL using distilled water as a solvent, and the experiments were carried out at the spontaneous pH of the solutions (pH = 6.3) containing CEF with a concentration of 5 ppm. Before the irradiation, the photoreactor was kept under dark conditions for 60 min to reach the adsorption–desorption equilibrium of CEF on the surface of photocatalytic nanoparticles. The reactor was irradiated by two visible light lamps (Beghelli, 8 W; wavelength emission in the range 400–800 nm). The lamps were positioned 15 cm above the upper surface of the batch reactor (Fig. S2). Moreover, the photoreactor was covered with a reflecting aluminum foil to keep only its upper surface under irradiation.

2.4.2. RPR

For the analysis of the influence of light modulation on the efficiency of CEF degradation, it was used a batch experimental setup equipped with a recirculating flat plate photocatalytic reactor (RPR) irradiated by a matrix of LEDs emitting visible light (in the range 400–800 nm) (Fig. 1).

The RPR was realized by the spin-off IPERA. It was designed with a flat geometry to increase the efficiency of the excitation of the structured photocatalyst, ensuring the homogeneity of the photon flux, and therefore the intensity of the incident light inside the reaction system [18].

The RPR features two separate compartments that operate independently. Each of them is provided with a Pyrex window which is transparent to visible light. A matrix of LEDs is positioned near the Pyrex windows, allowing the photocatalyst to be irradiated and avoiding the dispersion of light outside the system. It is fixed on a heatsink and connected to a digitally controlled LED driver. In particular, the light source consists of a single-layer aluminum printed circuit with dimensions of 30 × 15 cm, on which 240 LEDs are positioned, and arranged in 24 parallel rows of 10 LEDs spaced 1.05 cm. Furthermore, the LEDs are grouped in a series of strings, each of which is individually accessible through 12 connectors arranged on the sides of the board. Every string of LEDs is powered independently, and the light modulation is implemented by the LED driver. The LEDs used for the photocatalytic activity tests are CREE MLCAWT-H1-0000-000XE1. They irradiate a typical nominal luminous flux between 55.2 lm with a typical forward voltage drop between 3.5 V at 200 mA DC [15]. In detail, to evaluate the

incident light intensity on the surface of the structured photocatalyst inside the reactor a spectro-radiometer was used (StellarNet Inc).

The LED matrix was designed to optimize the uniformity of the light incident on the catalyst [24]. In particular, a triangular pattern with a 1.1 cm reticule distance was adopted.

A simplified experimental setup scheme is reported in Fig. 2. Specifically, the photocatalytic system used for the tests consists of an RPR (height = 200 mm; length = 100 mm; thickness = 10 mm), an LED matrix, an LED driver (Power Stage), a peristaltic pump for liquid recirculation, a tank containing the solution to be treated and a reactor cooling system.

CEF was initially spiked in distilled water and then in tap water to assess the effects of the nature of the contaminated aqueous matrix on the photodegradation. Table S1 lists the characteristics of the tap water used for the test.

In particular, the solution volume was 450 mL, and the experiments were carried out using a single reactor compartment at the spontaneous pH (6.3 and 7.34, in the case of using distilled and tap water matrix, respectively), with a CEF concentration of 5 ppm. The solution to treat has been placed in the tank. A recirculation flow of 28 mL min^{-1} has been realized by using the peristaltic pump. The liquid stream flowed over the surface of the structured photocatalyst and emerged from the top of the reactor, being collected in the tank which is equipped with a magnetic stirrer to guarantee the complete homogenization of the solution.

The LED matrix was designed in order to optimize the uniformity of the light incident on the catalyst. Considering the irradiance distribution of the single LED device as a Lambertian Emitter, it is possible to derive a design equation to obtain an ununiform irradiance distribution for several LED patterns [24].

The irradiance distribution is given by Eq. (1), where θ is the viewing angle, $E_0(r)$ is the irradiance (W m^{-2}) on the axis at distance r from LED, and m is defined by Eq. (2) from the view angle $\theta_{1/2}$ when the irradiance is half of the value at 0°.

For a triangular array between LEDs equal to d (Fig. S3 of Supplementary Material), the maximally flat condition at a distance z is given by Eq. (3).

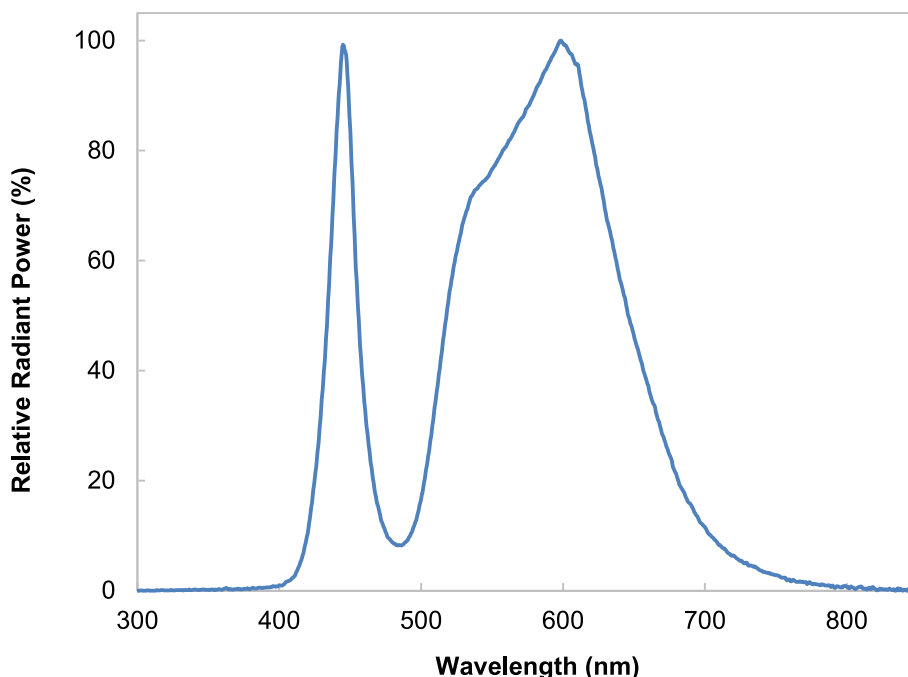$$E(r, \theta) = E_0(r)\cos^m\theta, \tag{1}$$

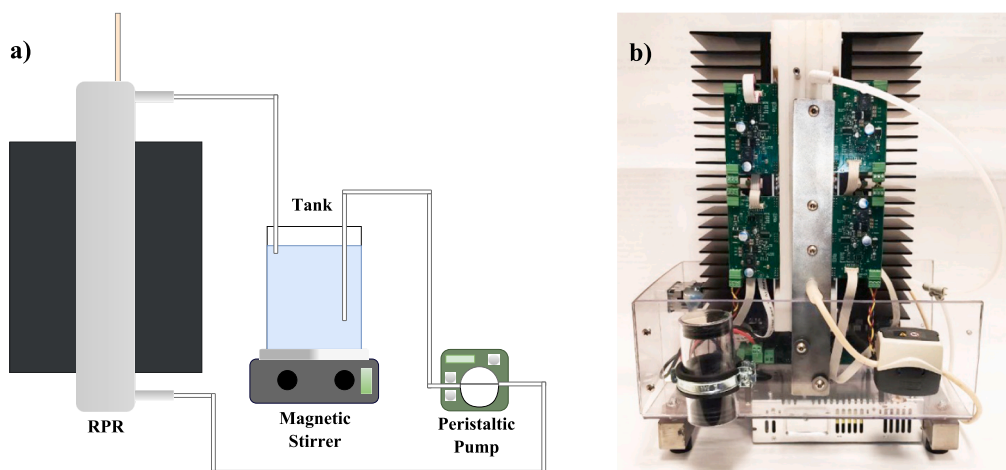**Fig. 1.** Emission spectrum of visible LEDs.

Fig. 2. A) experimental setup scheme; b) picture of the photoreactor.

$$m = -\frac{\ln 2}{\ln(\cos\theta_{1/2})} \tag{2}$$

$$d_0 = \sqrt{-\frac{1.2125}{m - 3.349^z}} \tag{3}$$

In the used setup, a triangular pattern with $d = 1.1$ cm reticle distance was adopted, producing, on the surface of the catalyst placed at a distance $z = 1$ cm, the irradiance plot shown in Fig. 3.

Fig. 4 shows the trend of the intensity of the incident light as a function of the average current fed to the LEDs. It is possible to observe the saturation effects due to the decrease in the reactivity/efficiency of the light source as the intensity of the supplied current increases [25]. This analysis underlines that it is not advantageous to power the light source with a current higher than 100 mA, as the luminous efficiency of the LEDs increases negligibly.

The detail of the light modulations tested in the RPR is reported in section SM1 and Fig. S4 of Supplementary Material.
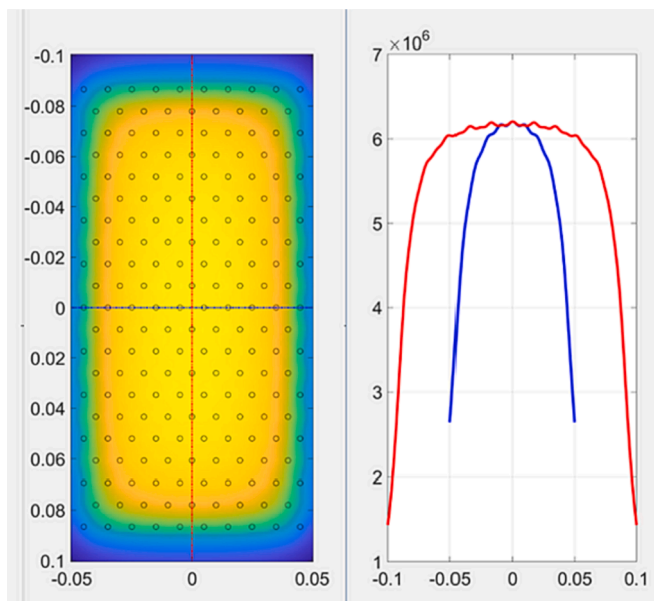

Fig. 3. Calculated light irradiance plot of LEDs matrix.

2.5. Analytical procedures

Each experimental test has been conducted for a total time of 240 min, including the initial interval of dark condition (dark phase) lasting the first 60 min. Then, the LEDs have been turned on (light phase), and, in the following 180 min, aqueous samples have been withdrawn. In detail, they were taken after 15 min, 30 min, 60 min, 120 min, and 180 min of irradiation time. The CEF residual concentration has been measured using a PerkinElmer UV–Vis spectrophotometer at a wavelength of 279 nm [26].

The total organic carbon (TOC) of aqueous solutions was measured by the high-temperature combustion method on a catalyst (Pt-Al$_2$O$_3$) in a tubular flow microreactor operated at 680 °C, with a stream of hydrocarbon-free air to oxidize the organic carbon [27].

A kinetic analysis of the photocatalytic degradation of CEF was carried out. The Langmuir–Hinshelwood model is usually used to describe the kinetics of the photocatalytic process [28]. The derivation is based on the degradation rate (r), which is expressed as follows:

$$r = \frac{dc}{dt} = \frac{k_r K_{ad} c}{1 + K_{ad} c} \tag{4}$$

where k_r, K_{ad}, and c are the kinetic constant, adsorption equilibrium constant, and concentration of antibiotic, respectively.

Considering that the concentration of pollutant is low, the equation above can be simplified to the first-order kinetics expression with an apparent degradation kinetic constant (k_{app}):

$$ln\left(\frac{c_0}{c}\right) = k_r K_{ad} c = k_{app} t \tag{5}$$

The value of the apparent degradation kinetic constant can be calculated by the slope of the straight line obtained from plotting $ln(c_0/c)$ vs. the irradiation time (t).

The TOC removal (mineralization) and CEF removal (degradation) efficiency at the generic irradiation time were evaluated using the following relationships:

$$TOC\ removal\ efficiency(t) = \left(1 - \frac{TOC(t)}{TOC_0}\right)100 \tag{6}$$

$$CEF\ removal\ efficiency(t) = \left(1 - \frac{C(t)}{C_0}\right)100 \tag{7}$$

where $TOC(t)$ is the total organic carbon at the generic irradiation time (ppm), TOC_0 is the initial total organic carbon (ppm), $C(t)$ is the CEF concentration at the generic irradiation time (ppm), C_0 is the initial CEF concentration (ppm).
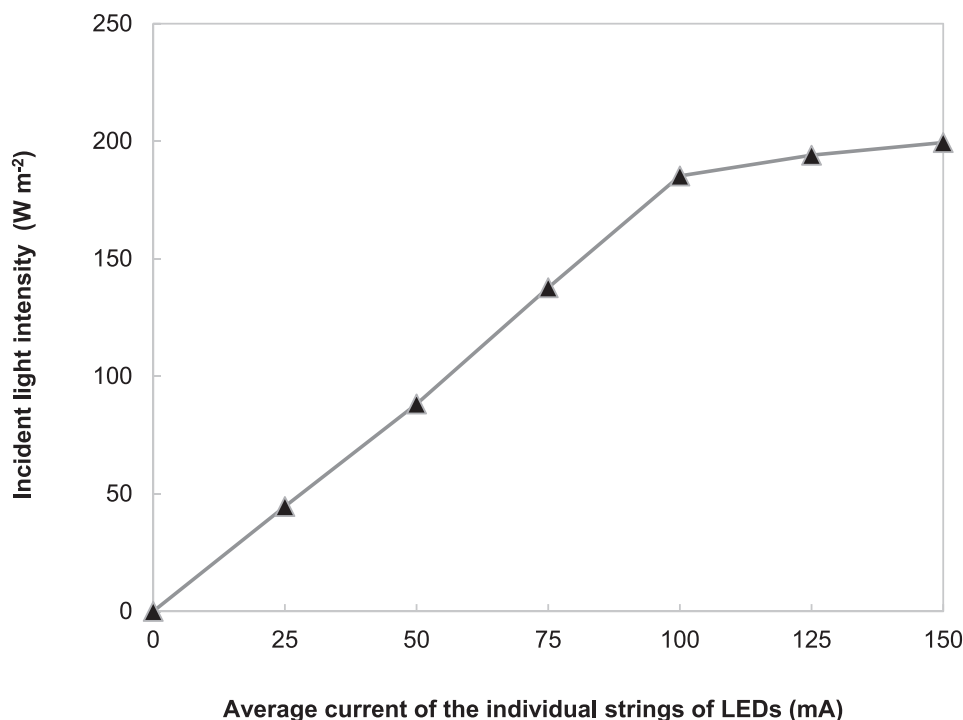
Fig. 4. Incident light intensity trend as a function of the average supply current of the LED string.

2.6. Ecotoxicological and genotoxicological test

The impact on survival of *A. franciscana* nauplii, metanauplii, juvenile and adults was evaluated after 48 h of exposure to different experimental conditions: initial solution spiked with Ceftriaxone (5 ppm; namely CEF), distilled water plus photocatalyst Fe-N-TiO$_2$/PS (namely Fe-N-TiO$_2$/PS), and solutions collected from treatment optimized with distilled water (S-VD$_{180}$) and with tap water (S-VD$_{TP}$) [29]. The experimental procedures for the hatching cysts and incubation of organisms with treatment were according to [30]. Two-way ANOVA followed by Tukey's test for multiple comparisons (GraphPad Prism Software version 9 for Windows, GraphPad Software, La Jolla, California, USA, https://www.graphpad.com) has been conducted to detect statistical significance of differences among different treatments, and controls.

Genotoxicity testing was performed using three larval stages and adult of *A. franciscana*. Specifically, four hundred nauplii and metanauplii, two hundred juvenile and 10 adults of *A. franciscana* were exposed to solutions collected from Fe-N-TiO$_2$/PS, S-VD$_{180}$, S-VD$_{TP}$. Collection of samples after 48 h, total RNA extraction and cDNA synthesis were performed according to [30]. The transcriptional expression of three heat shock protein (*hsp26*, *hsp60* and *hsp70*) and the normalized glyceraldehyde-3-phosphate dehydrogenase (*GAPDH*) were evaluated by Real Time qPCR. The RT-qPCR was performed following the manufacturer's instructions according to [30]. All experiments were performed in triplicates. The fold-change in relative expression was calculated using REST software [31,32]. The values above and below 2 were considered significant. The change in expression levels was represented through a Heatmap generated by GraphPad Prism Software.

3. Results and discussion

3.1. Photocatalyst characterization results

XPS measurements have been conducted on bare TiO$_2$ and Fe-N-TiO$_2$. From survey spectra (not reported) we have been able to distinguish the presence of Ti, O and C, in both samples, while N has been found only in Fe-N-TiO$_2$, as expected. Fe2p signal was not detected in the survey spectrum for the latter powder. Due to the absence of Fe2p signal and to the very low intensity of N1s signal, the chemical composition was calculated by HR spectra, to be more precise. High-resolution photoelectron regions gave important information related to the presence or absence of expected elements. Even integrating the Fe2p region signal for 3 h, a valuable signal that could be ascribed to the Fe2p doublet was not obtained (see Fig. 5d); this means that Fe, if present as expected, is at a lower concentration than XPS sensitivity (0.1 at. %) or it is somehow covered by a layer which is thicker than 10 nm (technique nominal analysis depth). N1s region has been, also, acquired for a long time (nearly one over and a half), and at the end, we got the signal reported in Fig. 5e, which corresponds to 0.4 at. %. The other HR regions, more well-defined, let us calculate the chemical composition, reported in Table 1. C, O and Ti values are close to each other, so no great differences can be appreciated.

Moving to the comparison between the common elements present in both samples, we can start from C1s region, reported in Fig. 5a. Both samples show the typical adventitious C shape, which includes: C-C/H (284.8 eV), C-O/N (286.4 eV) and C=O (288.9 eV) components (as reported also in Table 1) [33]. A new component has been found for the Fe-N-TiO$_2$ sample at 282.9 eV, which is usually assigned to C-C species due to defects or sp^1 structure. O1s region (Fig. 5b) shows two almost perfect overlapped curves, for both samples, in which we can infer the two components usually assigned to Ti-O species (530.0 eV) and the absorbed O (531.7 eV) [34]. The relative abundance of these two chemical shifts is reported in Table 1, as well. Also Ti2p doublet region (Fig. 5c) shows a perfect overlapping between the two experimental data for TiO$_2$ and Fe-N-TiO$_2$ powders. The shape of these doublets is the one reported in the literature for stoichiometric titania, with Ti2p$_{3/2}$ main peak located at 458.8 eV and its related Ti2p$_{1/2}$ peak at 5.7 eV apart, towards higher binding energy values [35]. This suggests that both N and Fe are not directly bonded to Ti, since no signal distortion has been revealed in the Ti2p region; moreover, no components are coming from the Ti region typical for Ti-N bond, at ~455 eV. If we rely on J. Du et al. work on N-doped TiO$_2$ nanocrystals [36], we can attribute the N1s chemical shift at 400.1 eV (see Fig. 5e) at an interaction between N and
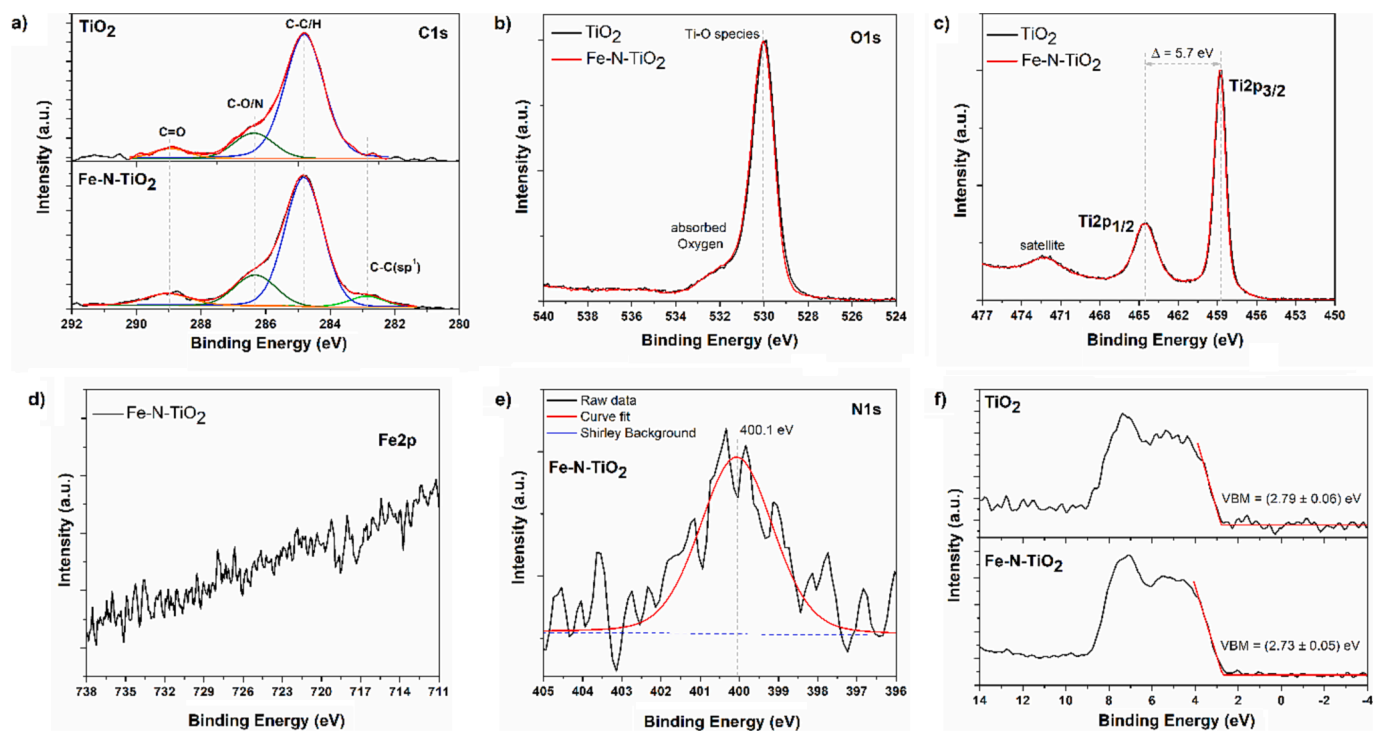
Fig. 5. XPS HR spectra related to a) C1s, b) O1s, c) Ti2p, d) Fe2p, e) N1s and f) Valence band regions.

Table 1
XPS analysis results. Relative atomic concentration (at.%), C1d and O1s chemical shifts from HR spectra deconvolution procedures and Valence Band Maximum (VBM) values calculated from VB HR region.

Relative atomic concentration [at.%]		
	TiO_2	$Fe-N-TiO_2$
C1s	18.8	18.1
O1s	58.1	58.1
Ti2p	23.1	23.4
N1s	–	0.4
Fe2p	–	–
C1s chemical shift [area %]		
C (sp^1)	–	6.1 ± 1.1
C-C/H	79.2 ± 1.4	69.2 ± 1.3
C-O/N	15.1 ± 2.7	17.0 ± 2.5
C = O	5.7 ± 1.1	7.7 ± 1.4
O1s chemical shift [area %]		
Ti-O	87.6 ± 1.7	85.5 ± 1.7
–OH	12.4 ± 2.2	14.5 ± 2.3
Valence band region [eV]		
VBM	2.79 ± 0.06	2.73 ± 0.05

O, in a titanium matrix, which would create, at the same time, a chemical shift in the O1s region, which overlaps with the one already found for absorbed O species. In [37] they also have not found any modification induced in the Ti2p region according to Fe inclusion in the TiO_2 matrix. A last check has been dedicated at the valence band peak, to observe if the introduction of N and Fe atoms has modified somehow the region, which represents the experimental counterpart of the theoretical DOS (Density of States). First of all, the shape of both curves (Fig. 5f) is like the one reported in the literature for pure titania [38]. So we calculated the Valence Band Maximum (VBM) position, referred to the Fermi Level ($E_F = 0$ eV), by means of a linear curve fit in the descending portion of the signal, towards 0 eV. We obtained two values (see Fig. 5f and Table 1), which are quite similar (2.79 ± 0.06 eV and 2.73 ± 0.05 eV, respectively), considering the uncertainty of the method applied to obtain them. This means that the inclusion of the two atoms, Fe and N, in the structure of the titania has not brought about evident

changes in the valence band region.

Photoluminescence (PL) spectroscopy is a widely used non-destructive optical characterization technique to probe the doping effect of a semiconductor, as it can provide valuable information on both intrinsic and extrinsic transitions. In particular, the photoluminescence signal in the relaxation process, resulting from the recombination of free charge carriers, can be quenched due to charge trapping sites [39].

Fig. 6 shows the PL spectra of bare TiO_2 and $Fe-N-TiO_2$ samples excited by 362 nm light. The profile of the emission curves, recalls that obtained by Selvam et al. [40] with the peaks located at 425 nm and 490 nm. An additional peak can be noticed at 530 nm [41]. The listed peaks are all attributed to the charge-transfer transition of oxygen vacancy-trapped electrons to the valence band of TiO_2. In particular, the latter two are attributed to the oxygen vacancy with two trapped electrons, i.
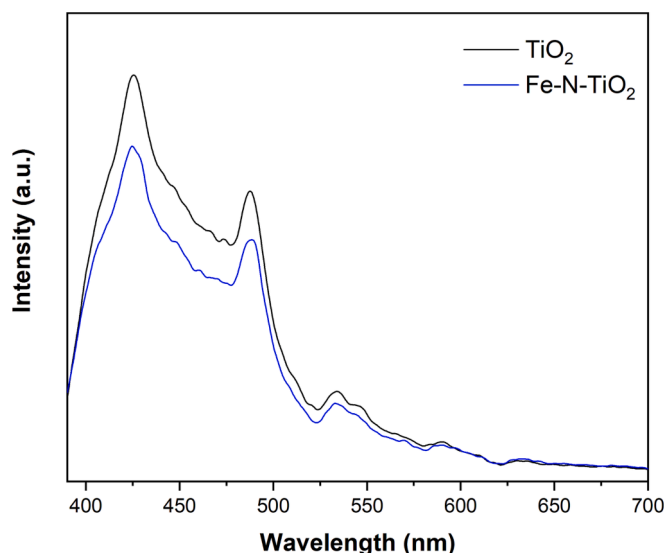

Fig. 6. Photoluminescence spectra of bare TiO_2 and $Fe-N-TiO_2$.

e., F center, and to the oxygen vacancy with one trapped electron, i.e., F^+ center, at 490 and 530 nm, respectively [41,42]. The quenching of the PL intensity in the Fe-N-TiO$_2$ sample can be attributed to a lower recombination rate of electron-hole pairs (e^-/h^+) in the doped sample [43].

Fig. 7 reports the Raman spectra of the bare PS plate and the Fe-N-TiO$_2$/PS photocatalyst. From the results it can be seen that the spectrum of the structured photocatalyst presents only the primary bands typical of TiO$_2$ in the anatase phase (at 144, 397, 516, and 638 cm^{-1}) [44], indicating that Fe-N-TiO$_2$ particles uniformly cover the PS surface. It should be emphasized that the Raman analysis of the structured photocatalyst was conducted on different surface points. In particular, the analyzed points are indicated in Fig. S6, obtaining in all cases the same Raman signals.

UV–Vis DRS results (Fig. 8) showed that the PS absorbs mainly in the UV region, in agreement with the literature [45]. As expected, the main absorption edge of TiO$_2$/PS lies in the range 390–400 nm (UV region) [21]. On the other hand, for the Fe-N-TiO$_2$/PS, a redshift of absorption onset was observed due to the presence of Fe-N-TiO$_2$ photocatalyst on the PS surface.

3.2. Photocatalytic activity results with the SPR

Initially, the tests were conducted using the experimental setup with the SPR. In particular, three tests were carried out: a photolysis test and two photocatalytic activity tests with TiO$_2$ and Fe-N-TiO$_2$ powders using a dosage equal to 3 g/L. The results, shown in Fig. 9, highlighted that photolysis alone and the photocatalytic process with the undoped titania did not lead to the degradation of the CEF whereas the Fe-N-TiO$_2$ photocatalyst in powder is effective in pollutant removal. Indeed, the almost complete CEF degradation was achieved after 60 min of visible light irradiation.

3.3. Photocatalytic activity results with the RPR: stability tests of the Fe-N-TiO$_2$/PS structured photocatalyst

After studying the degradation activity of the CEF with the Fe-N-TiO$_2$ in powder form, experimental tests were carried out to confirm the stability of the structured photocatalyst using the RPR (Fig. 10). These tests were conducted using FD light modulation, powering each string of LEDs with an average electric current equal to 100 mA, since for this value of I_{avg} the saturation of the incident light intensity was reached (185 ± 5 W m^{-2}). The results confirmed the stability of the structured photocatalyst. Indeed, for the various tests, the behavior of the pollutant concentration as a function of the irradiation time was similar (Fig. 10a) with a value of CEF removal efficiency after 180 min of visible light of about 65 % and showing a value of apparent kinetic degradation
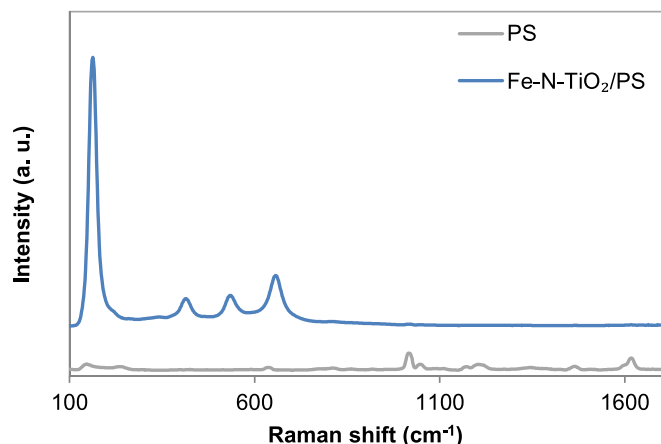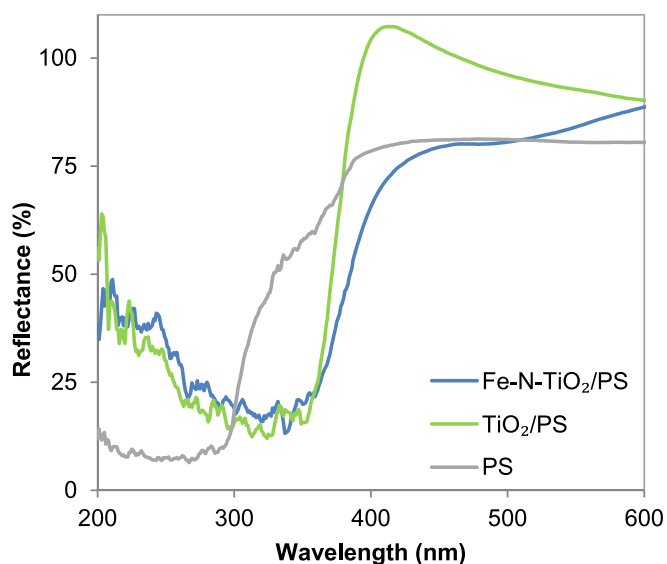

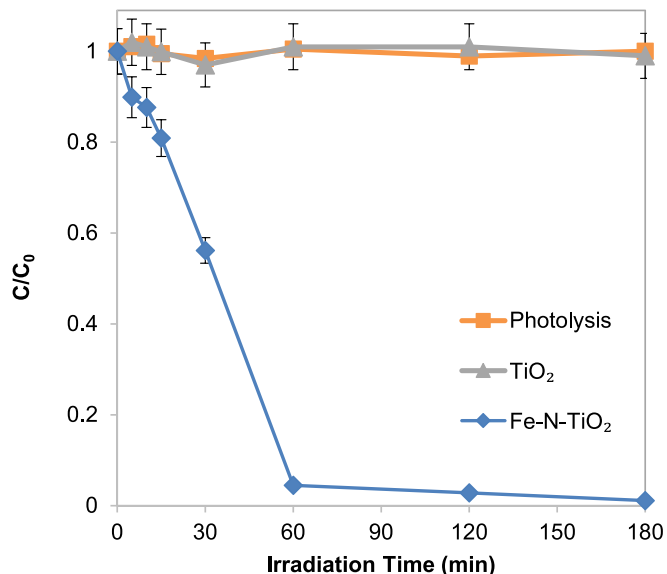**Fig. 8.** UV–Vis DRS of PS plate and Fe-N-TiO$_2$/PS photocatalyst.

Fig. 9. CEF degradation under visible light by photolysis and photocatalysis using TiO$_2$ and Fe-N-TiO$_2$ powders in the experimental setup with the SPR.

constant equal to about 0.006 min^{-1} in all the reused cycles (Fig. 10b). Furthermore, the reaction system allowed also the mineralization of the pollutant since an average value of TOC removal of about 60 % was obtained after 180 min of irradiation time (Fig. 10c).

3.4. Photocatalytic activity results with the RPR: Influence of the incident light intensity

Photocatalytic tests were carried out to analyze the influence of the incident light intensity on the photocatalytic activity of RPR. For this purpose, the degradation of CEF was analyzed using visible light irradiation at fixed duty LED dimming (FD). The average current flowing in each individual LED string, I_{AVG} was fixed in the range of 25–100 mA to obtain different values of incident light intensity ($44 \pm 5 - 185 \pm 5$ W m^{-2}) (Fig. S4). The experimental results, shown in Fig. S5, evidenced that with the increase of I_{AVG} from 20 to 50 mA, the kinetic constant of CEF degradation linearly increased, while for higher values it (75 – 100 mA) did not show a significant increase. This result can be attributed to

Fig. 7. Raman spectra of PS plate and Fe-N-TiO$_2$/PS photocatalyst.
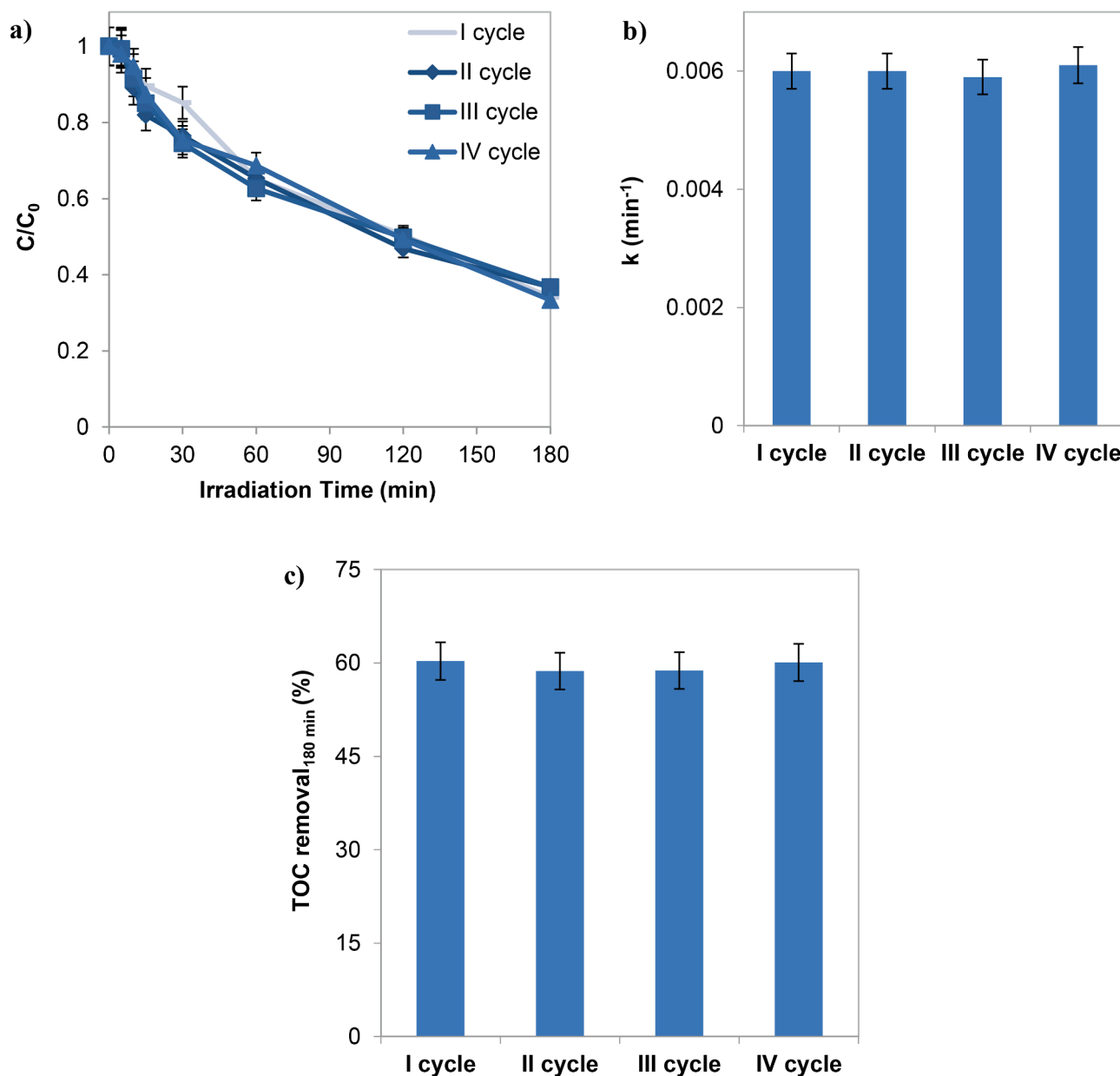
Fig. 10. a) degradation of CEF under visible light obtained with fd light modulation for five reuse cycles; b) values of apparent kinetic degradation constant for CEF degradation obtained with fd light modulation for five reuse cycles; c) TOC removal obtained after 180 min of irradiation with FD light modulation for five reuse cycles.

the decrease in the reactivity/efficiency of the LEDs, and to the recombination reaction of the photoexcited pairs being favored as the intensity of the electric current with which the light source is supplied increases [16,46]. For this reason, the tests of photocatalytic activity with the other LED dimming modulations were realized by feeding the LEDs with an I_{AVG} equal to 50 mA.

### 3.5. Photocatalytic activity results with the RPR: Influence of the period (T) and amplitude (A)

Experimental tests were carried out to test the influence of period (T) and amplitude (A) on the sinusoidal modulation of light (S-VD).

The period of modulated light corresponds to the time interval between two maximum peaks of the average current fed to the light source and, therefore, of the incident light intensity. The amplitude of the modulated light is defined as the difference between the maximum peak and minimum peak of the average current fed to the light source.

Fig. 11 shows the trend of the average electric current with which the LEDs are powered during the irradiation time, for a value of T and A fixed at 30 s and 100 mA ($I_{AVG\ min} = 0$ mA, $I_{AVG\ max} = 100$ mA) respectively.

The tests for evaluating the photocatalytic activity as a function of the amplitude of the S-VD light modulation were carried out by setting the period value to 30 s and fixing a specific value for the minimum and maximum average current ($I_{AVG\ min}$ and $I_{AVG\ max}$, respectively), and therefore also of a minimum and maximum value of the intensity of the incident light (Φ_{min} and Φ_{max}, respectively). The amplitudes examined for S-VD light modulation were the following: 20 mA ($I_{AVG\ min} = 40$ mA, and $I_{AVG\ max} = 60$ mA), 50 mA ($I_{AVG\ min} = 25$ mA, and $I_{AVG\ max} = 75$ mA), and 100 mA ($I_{AVG\ min} = 0$ mA, and $I_{AVG\ max} = 100$ mA). The results obtained show that the variation of the amplitude of the sinusoidal modulation significantly affected the photodegradation of the CEF and the maximum value of the apparent kinetic degradation constant of the pollutant (0.0082 min^{-1}) was recorded for the amplitude of 50 mA.
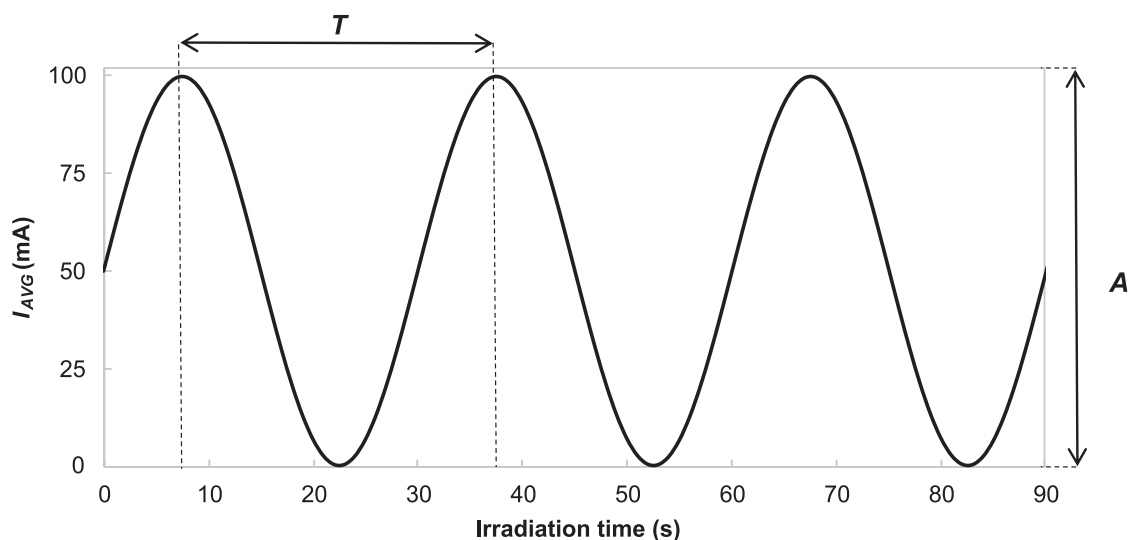
Fig. 11. The trend of the average electrical current powered to the light source as a function of the irradiation time for the S-VD light modulation with $T = 30$ s, $A = 100$ mA, $I_{AVG\ min} = 0$ mA, and $I_{AVG\ max} = 100$ mA.

Indeed, as shown in Fig. 12, for this amplitude value an 18 % increase in the removal efficiency of the CEF after 180 min of sinusoidal modulated visible light was recorded.

Further tests were conducted to evaluate the influence of the period on the photocatalytic process using S-VD modulation with optimal amplitude ($A = 50$ mA, $I_{AVG\ min} = 25$ mA, and $I_{AVG\ max} = 75$ mA).

Fig. 13 showed that the optimal period of S-VD modulation was equal to 30 s; this modulation showed the highest value of the CEF removal efficiency (equal to 75 %), compared to the values of 60 %, 61 %, and 59 %, achieved for the S-VD modulation with the period of 3 s, 20 s and 60 s, respectively. From the experimental results emerged that the optimal S-VD modulation is characterized by an amplitude of 50 mA and a period of 30 s.

Comparing the pollutant concentration trend of the optimal S-VD modulation with the fixed light modulation with electric current fed to the LEDs of 50 mA, an increase in the CEF removal efficiency of about 45 % was observed (Fig. 14). This enhancement of photocatalytic activity can be justified by the fact that the sinusoidal modulation of the incident light intensity allows to decrease the rate of the photo-excited pairs recombination phenomena, as evinced by kinetic modeling reported in the literature, developed for the photocatalytic degradation of an organic model pollutant (terephthalic acid) using the photocatalysis with modulated visible light LEDs [16].
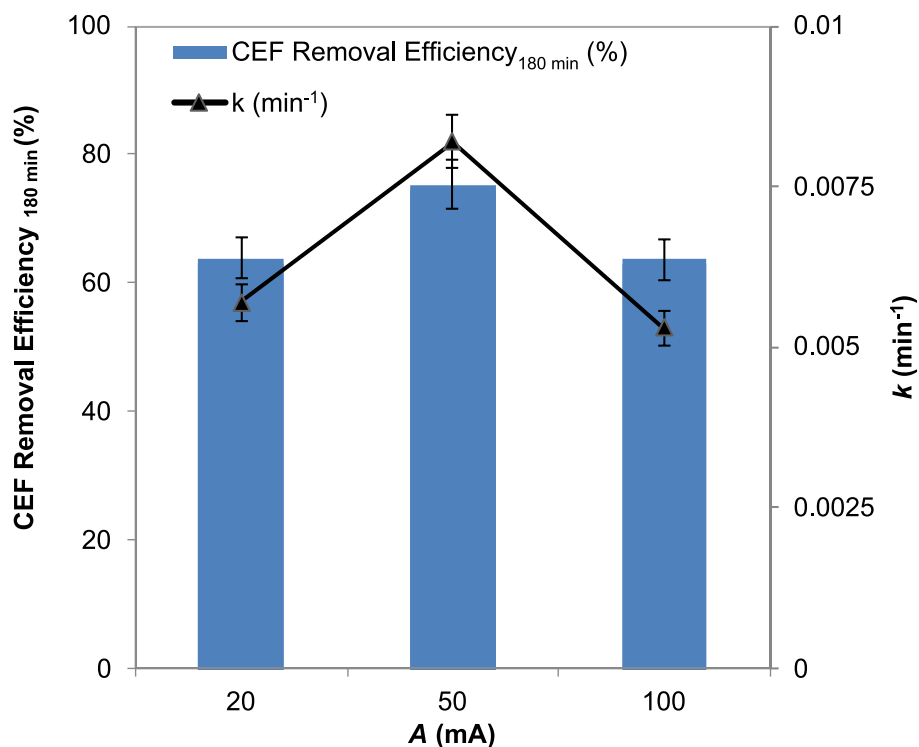
Fig. 12. Apparent kinetic degradation constant and CEF removal efficiency after 180 min of sinusoidal modulated visible light as a function of the amplitude for S-VD modulation of light ($T = 30$ s, $A = 100$ mA, $I_{AVG\ min} = 0$ mA, and $I_{AVG\ max} = 100$ mA).
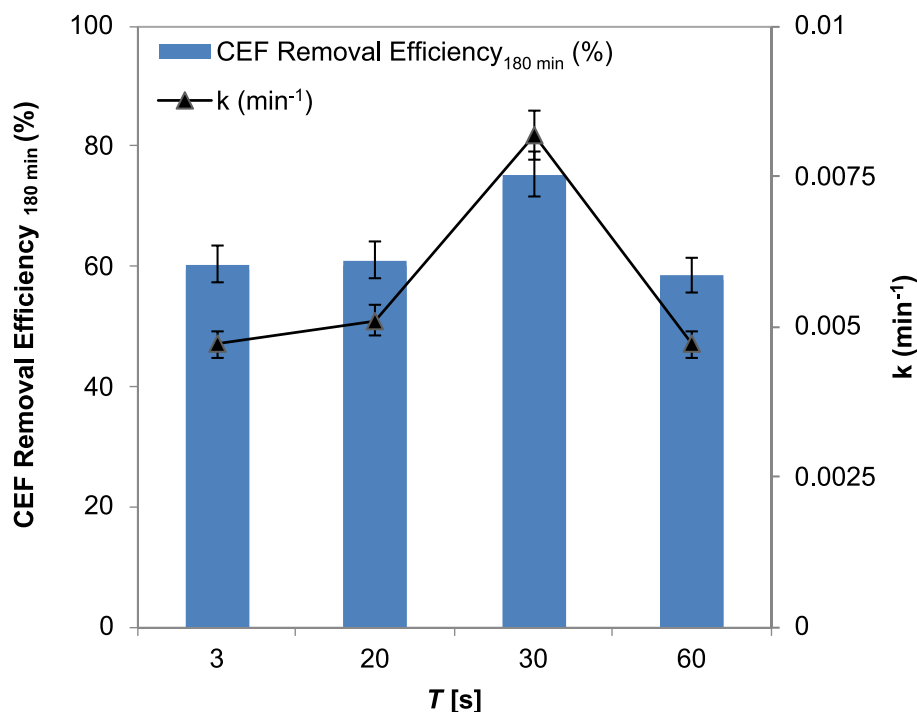
Fig. 13. Apparent kinetic degradation constant and CEF removal efficiency after 180 min of sinusoidal modulated visible light as a function of the period for S-VD modulation of light.
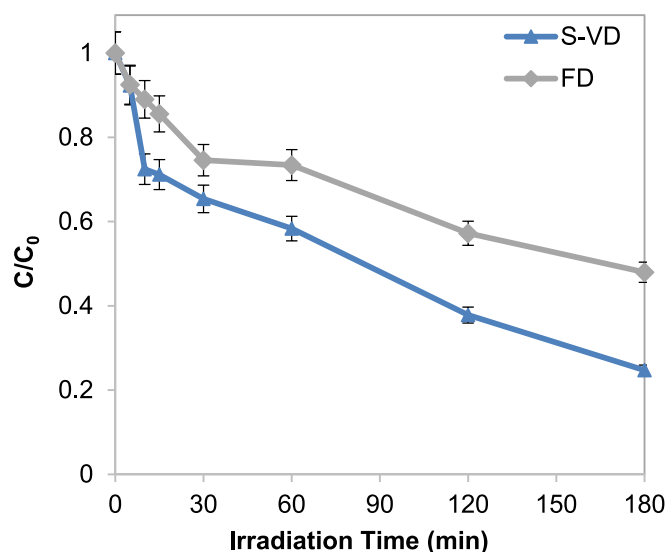

Fig. 14. Behaviour of CEF relative concentration as a function of irradiation time for FD modulation ($I_{AVG} = 50$ mA) and for the optimal S-VD modulation ($T = 30$ s, $A = 50$ mA, $I_{AVG\ min} = 25$ mA, and $I_{AVG\ max} = 75$ mA).

3.6. Photocatalytic activity results with the RPR: Influence of the different light modulations

Several tests were conducted to analyze the influence of the different light modulations on the photocatalytic activity of the reaction system. The modulations studied were the following: triangular variable duty-cycle (T-VD) (triangular variable irradiation), square wave variable duty-cycle (SW-VD) (square wave variable irradiation), saw-tooth variable duty-cycle (ST-VD) (sawtooth variable irradiation), pulse variable duty-cycle (P-VD) (pulse variable irradiation), and pseudo-sinusoidal variable duty-cycle (PS-VD) (pseudo-sinusoidal variable irradiation). They have been evaluated by supplying an average current between 25

and 75 mA ($\Phi_{min} = 44 \pm 5$ W m^{-2} and $\Phi_{max} = 138 \pm 5$ W m^{-2}) with a period equal to 30 s, in order to use the optimal amplitude and period individuated for the S-VD light modulation in previous tests.

Fig. S7 (Supplementary Material) shows the trend of CEF relative concentration as a function of irradiation time for the different light modulations. The optimal modulation for the photodegradation of the pollutant was the S-VD light modulation since the highest value of CEF degradation was obtained (75 %).

Furthermore, as shown in Fig. 15, the results showed that the reaction system tested with the various modulations succeeds not only in degrading the pollutant but also in its mineralization. In particular, the highest TOC removal value after 180 min of visible light, equal to 70 %, and the highest apparent degradation kinetic constant (0.0082 min^{-1}) was achieved with S-VD modulation.

3.7. Photocatalytic activity results with the RPR: effect of water matrix nature

It has been reported that the inorganic ions present in the water to be treated may have an impact on the photocatalytic performances [47–49]. For this reason, an additional test using the optimal light modulation (S-VD, $T = 30$ s, $\Phi_{min} = 44 \pm 5$ W m^{-2}, and $\Phi_{max} = 138 \pm 5$ W m^{-2}) was carried out using a tap water sample (whose characteristics are reported in Table S1 of Supplementary Material) contaminated by CEF, to evaluate the water matrix effect.

The results reported in Fig. 16 show the effectiveness of the system in the CEF degradation (Fig. 16a) and mineralization (Fig. 16b) also with tap water. Indeed, the TOC removal obtained was 75 % and 72 %, for the tests using distilled and tap water, respectively.

However, for the test conducted with the tap water matrix, the apparent kinetic constant slightly decreased (Fig. 16b) resulting lower (11 %) than the test conducted with distilled water. This result can be attributed to the ions present in tap water, which act as radical scavengers for the photogenerated ROS during the photocatalytic reaction [50].
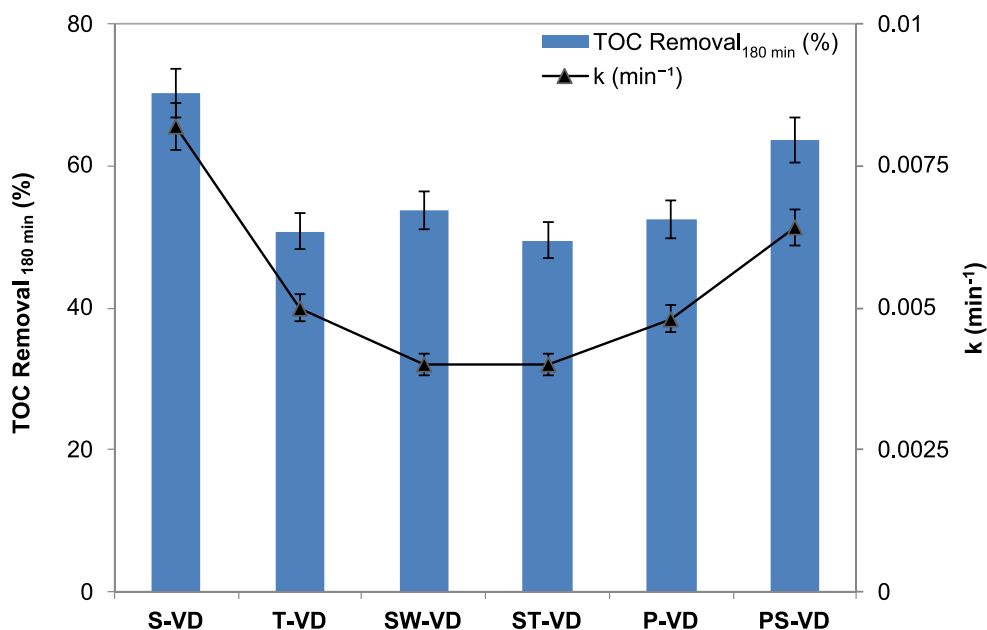
Fig. 15. CEF apparent kinetic degradation constant values, and TOC removal after 180 min of visible light using the following modulations: S-VD, T-VD, SW-VD, ST-VD, P-VD, and PS-VD, with $A = 50$ mA, $T = 30$ s, $I_{AVG\,min} = 25$ mA, and $I_{AVG\,max} = 75$ mA.
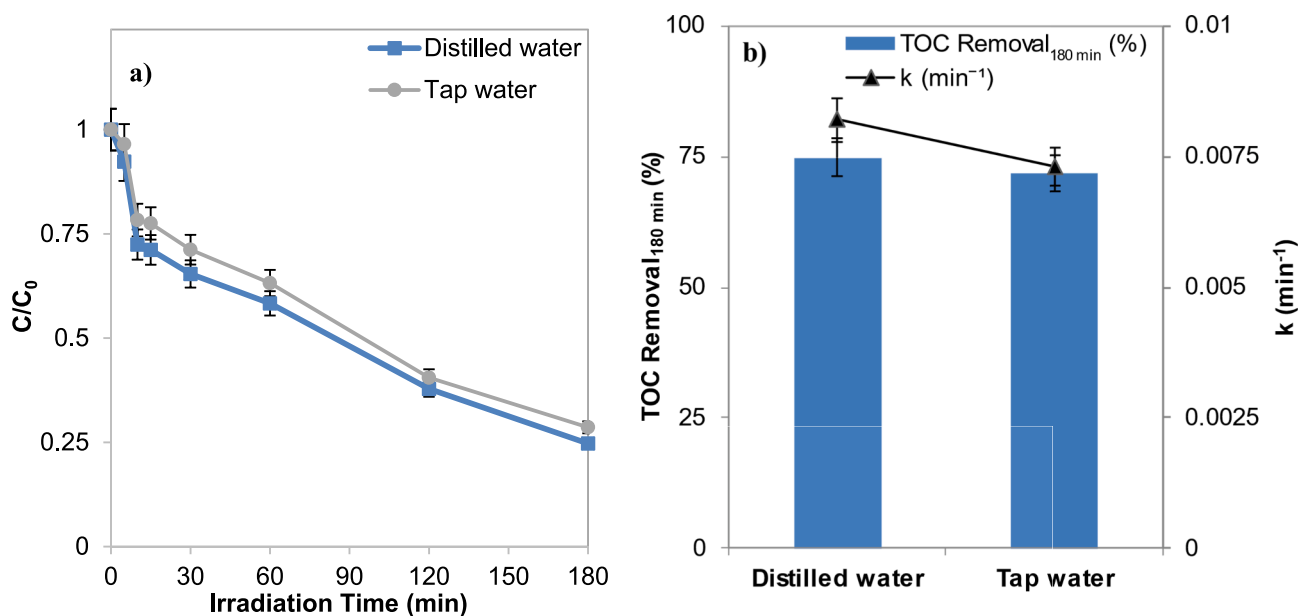

Fig. 16. a) trend of CEF relative concentration as a function of irradiation time; b) apparent kinetic degradation constant, and TOC removal after 180 min of visible light irradiation for the tests conducted using the optimal modulation (S-VD, with $A = 50$ mA, $T = 30$ s, $I_{AVG\,min} = 25$ mA, and $I_{AVG\,max} = 75$ mA) in presence of distilled and tap water.

3.8. Photocatalytic activity results with the RPR: electric energy consumption evaluation

Following the experimental tests, the electric energy consumption related to the photodegradation of 90 % of CEF in 1 m³ of contaminated water was evaluated for the tests conducted with average incident intensity light on the structured photocatalyst of 88 ± 5 W m^{-2}. This analysis was performed using the correlation of Bolton et al. [51]:

$$E_{E/O} = \frac{P t_{90\%} 1000}{V 60 \ln\left(\frac{c(t_0)}{c(t)}\right)}$$ (8)

where P is the nominal power of the light source (kW), $t_{90\%}$ is the irradiation time to obtain a 90 % removal of CEF (min), V is the solution volume treated (L), $c(t_0)$ is the CEF concentration at the initial irradiation time (ppm), and $c(t)$ is the CEF concentration at the irradiation time t (min).

The values of electric energy consumption obtained by the experimental data collected for the different light modulations are shown in Fig. 17.

The calculated values of $E_{E/O}$ underline that the S-VD modulation allowed a reduction of about 51 % in the electric energy consumption compared to SW-VD and ST-VD light modulation techniques.

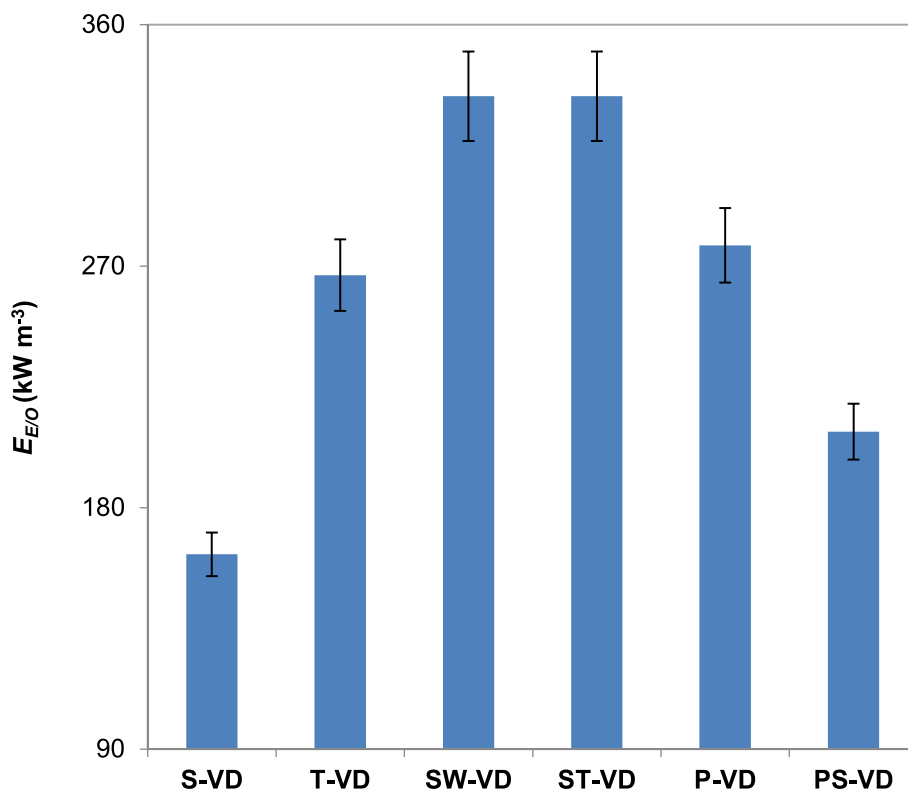From the data reported in literature papers dealing with the

Fig. 17. Histogram of electric energy consumption values for the reduction of 90 % of the CEF in 1 m^3 of solution for the following light modulation: S-VD, T-VD, SW-VD, PS-VD, with $A = 50$ mA, $T = 30$ s, $I_{AVG\ min} = 25$ mA, and $I_{AVG\ max} = 75$ mA.

photocatalytic degradation of CEF, it was possible to identify the value of the degradation kinetic constant and calculate the electricity energy consumption required for the 90 % reduction of CEF in 1 m^3 using the Eq. (8). The obtained values are compared with that obtained in the present work using the optimal light modulation (S-VD, $A = 50$ mA, $T = 30$ s, $I_{AVG\ min} = 25$ mA, and $I_{AVG\ max} = 75$ mA). The results are reported in Table 2, showing that our photocatalytic system presents the lowest electric energy consumption.

Therefore, the use of light modulation allows the intensification of the CEF photodegradation process under visible irradiation since the light modulation allows to reduce the electric energy consumption.

3.9. Ecotoxicity and genotoxicity evaluation

As shown in Fig. 18, ceftriaxone untreated solution (5 ppm) caused 100 % of mortality (about 10–20 %) in all life stages that was statistically significant respecting to control (p < 0.0001).

Considering the treated solutions, the treatments (both the one optimized in distilled water (S-VD$_{180}$) and the one optimized in tap water (S-VD$_{TP}$) greatly reduce the toxicity of the starting CEF solution

Table 2
Comparison of the electric energy consumption for the reduction of 90 % of the CEF in 1 m^3 of solution with the optimal sinusoidal light modulation and the other works reported in the literature.

| Photocatalytic system	Photocatalyst	P [kW]	k [min^{-1}]	V [L]	$E_{E/O}$ [kWh m^{-3}]
Present work	Fe-N-TiO$_2$/PS	0.036	0.0082	0.45	163
[8]	Bi$_2$WO$_6$/g-C$_3$N$_4$	0.3	0.0232	0.1	2158
[28]	CdS-g-C$_3$N$_4$	0.3	0.0336	0.1	1488
[8]	Bi$_2$WO$_6$ nanoflowers	0.3	0.0049	0.1	10,204
[52]	CeO$_2$/ZnO	0.018	0.011	0.075	364

for all *Artemia* stages, and in most cases, it could be considered as residual toxicity due to the presence of Fe-N-TiO$_2$/PS.

Specifically, these treatments caused about 40 % and 30 % of mortality in nauplii and metanauplii (Fig. 18a-b), and in juvenile and adult (Fig. 18c-d). Similarly, after 48 h of exposure to aqueous solutions of Fe-N-TiO$_2$/PS, a significant increase of about 30 % of mortality in nauplii, metanauplii, juvenile and adult was observed. All these data were statistically significant respecting only to the control and ceftriaxone solutions (p < 0.0001). Since after exposure with treated effluent (S-VD$_{180}$ and S-VD$_{TP}$), we observed similar effects reported in aqueous solutions of Fe-N-TiO$_2$/PS, it could be considered residual toxicity due to the presence of Fe linked to possible leaching of a small quantity of Fe-N-TiO$_2$ from the PS plate, which however did not affect the stability of Fe-N-TiO$_2$/PS structured photocatalyst.

Molecular investigations on *A. franciscana* three larval stages and adult are shown in Fig. 19. To clarify the role of Fe-N-TiO$_2$/PS in *Artemia* toxicity, the relative expressions of *hsp26, hsp60* and *hsp70* genes were evaluated.

The analyzed solutions were able to switch on the expression levels of almost all genes analyzed, (in red and green up-regulated and down-regulated genes, respectively; Fig. 19). In particular, Fe-N-TiO$_2$/PS, S-VD$_{180}$ and S-VD$_{TP}$ i) down-regulated *hsp26* in all life stages, *hsp60* and *hsp70* in nauplii; ii) up-regulated *hsp70* genes in metanauplii; and iii) only S-VD$_{180}$ was able to decrease the expression level of *hsp60* in metanauplii (Fig. 19). For more details about the values, see also Table S2 of Supplementary Material.

The molecular results were in according with morphological data, showing similar results both for the photocatalyst and two different treatments. Based on these observations, it could be considered the residual presence of Fe particles activates the molecular pathway involved in stress response, which in turn may induce changes in physiological mechanisms, and consequently the mortality. The heat shock proteins (especially *hsp70* and *hsp26*) are important in the immune response and protein protection from irreversible denaturation against subsequent
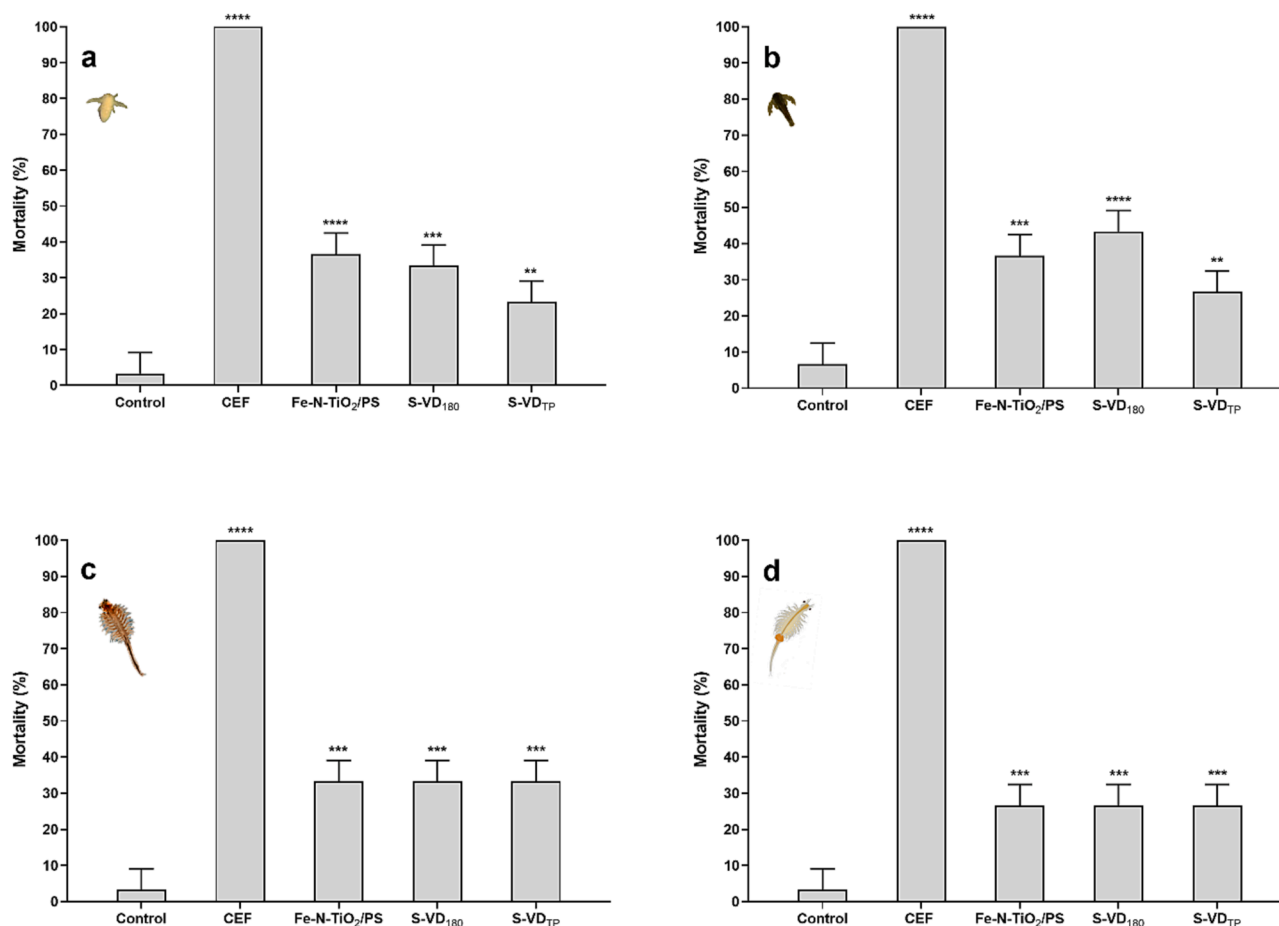
Fig. 18. Percentage of dead (a) nauplii, (b) metanauplii, (c) juvenile and (d) adult after 48 h of exposure to Fe-N-TiO$_2$/PS solution (distilled water + Fe-N-TiO$_2$), Ceftriaxone solution (5 ppm), Ceftriaxone + Fe-N-TiO$_2$/PS (Treated effluents after 180 min of visible light irradiation optimized with distilled water (S-VD180) and tap water (S-VDTP)). Data are reported as a mean ± standard deviation. Two-way ANOVA by Tukey's test (* $p < 0.05$, ** $p < 0.01$, *** $p < 0.001$, **** $p < 0.0001$).
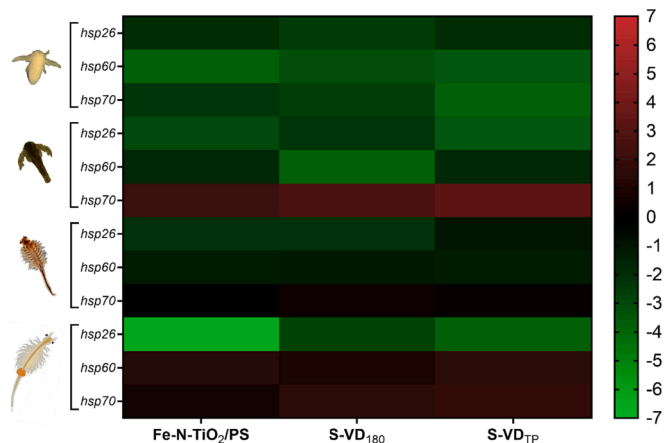
Fig. 19. Heatmaps shows expression profiles of the three genes analysed by Real Time qPCR in organisms exposed distilled water + Fe-N-TiO$_2$/PS (Fe-N-TiO$_2$), Ceftriaxone + Fe-N-TiO$_2$/PS (Treated effluents after 180 min of visible light irradiation optimized with distilled water (S-VD180) and tap water (S-VDTP)). Red, green and black colours represent up-regulated, down-regulated and no-regulated (no variation in expression) genes with respect to the control. (For interpretation of the references to colour in this figure legend, the reader is referred to the web version of this article.)

deleterious environmental stresses [53–56]. For these reasons, these genes are considered as "defensome" toward toxicants in these crustaceans [57].

4. Conclusions

This work was aimed at studying the influence of controlled modulation of visible light emitted by LEDs on the performances of a flat plate photocatalytic reactor for CEF degradation in the presence of Fe-N-TiO$_2$ immobilized on a PS plate (Fe-N-TiO$_2$/PS). The structured photocatalyst (Fe-N-TiO$_2$/PS) was successfully prepared by solvent-assisted method. Physical-chemical properties confirmed the presence of Fe-N-TiO$_2$ particles on the PS surface and their uniform distribution on the polymer support. The light irradiation of the flat plate photoreactor has been modulated over time using the dimming duty-cycle modulation techniques, improving the overall process efficiency. The optimal light modulation was the sinusoidal variable duty-cycle modulation (S-VD), which resulted in a 75 % CEF degradation and TOC removal of about 70 %, after 180 min of irradiation time (apparent degradation kinetic constant equal to 0.0082 min^{-1}). Interestingly, the efficiency of the photocatalytic system (using the optimal S-VD light modulation) was largely preserved also in the presence of tap water.

Finally, the photocatalytic system presented energy consumption significantly lower than that of those required by catalytic systems studied in the literature dealing with CEF photocatalytic degradation. Treatments with Fe-N-TiO$_2$/PS in both distilled water (S-VD180) and tap water (S-VDTP) significantly reduced the toxicity. Therefore, the irradiation of Fe-N-TiO$_2$/PS by LEDs light modulation techniques in a flat

plate photoreactor could be considered as an appropriate treatment of CEF-contaminated wastewater. Moreover, the study emphasizes the importance of understanding both morphological and molecular impacts when assessing environmental toxicity, shedding light on the intricate interplay between contaminants and treated effluents.

CRediT authorship contribution statement

Nicola Morante: Writing – original draft, Methodology, Investigation, Formal analysis, Data curation. **Olimpia Tammaro:** Writing – original draft, Methodology, Investigation, Data curation. **Luisa Albarano:** Writing – original draft, Methodology, Investigation, Formal analysis, Data curation. **Luca De Guglielmo:** Writing – original draft, Investigation, Formal analysis, Data curation. **Nunzio Oliva:** Writing – original draft, Investigation, Data curation. **Olga Sacco:** Writing – original draft, Supervision, Methodology, Investigation, Conceptualization. **Antonietta Mancuso:** Writing – original draft, Investigation, Formal analysis, Data curation. **Micaela Castellino:** Writing – original draft, Methodology, Investigation, Data curation. **Diana Sannino:** Writing – review & editing, Visualization, Investigation. **Nicola Femia:** Writing – original draft, Methodology, Investigation, Formal analysis, Data curation. **Giusy Lofrano:** Writing – review & editing, Methodology, Investigation, Formal analysis. **Giovanni Libralato:** Writing – review & editing, Investigation, Formal analysis, Data curation. **Serena Esposito:** Writing – review & editing, Methodology, Investigation, Data curation, Conceptualization. **Vincenzo Vaiano:** Writing – review & editing, Validation, Supervision, Methodology, Data curation, Conceptualization.

Declaration of competing interest

The authors declare that they have no known competing financial interests or personal relationships that could have appeared to influence the work reported in this paper.

Data availability

Data will be made available on request.

Acknowledgements

Appendix A. Supplementary data

Supplementary data to this article can be found online at https://doi.org/10.1016/j.cej.2024.149175.

References

[1] E.T.E.F.o.P.I.a. Associations, The Pharmaceutical Industry: A Key Asset To Scientific And Medical Progress, 2022.

[2] M. Ortúzar, M. Esterhuizen, D.R. Olicón-Hernández, J. González-López, E. Aranda, Pharmaceutical pollution in aquatic environments: a concise review of environmental impacts and bioremediation systems, Front. Microbiol. 13 (2022) 869332.

[3] M. Patel, R. Kumar, K. Kishor, T. Mlsna, C.U. Pittman Jr, D. Mohan, Pharmaceuticals of emerging concern in aquatic systems: chemistry, occurrence, effects, and removal methods, Chem. Rev. 119 (6) (2019) 3510–3673.

[4] G. Lofrano, R. Pedrazzani, G. Libralato, M. Carotenuto, Advanced oxidation processes for antibiotics removal: a review, Curr. Org. Chem. 21 (12) (2017) 1054–1067.

[5] E.Y. Klein, T.P. Van Boeckel, E.M. Martinez, S. Pant, S. Gandra, S.A. Levin, H. Goossens, R. Laxminarayan, Global increase and geographic convergence in antibiotic consumption between 2000 and 2015, Proc. Natl. Acad. Sci. 115 (15) (2018) E3463–E3470.

[6] S. Li, B.S. Ondon, S.-H. Ho, J. Jiang, F. Li, Antibiotic resistant bacteria and genes in wastewater treatment plants: From occurrence to treatment strategies, Sci. Total Environ. 838 (2022) 156544.

[7] C. Cai, H. Liu, B. Wang, Performance of microwave treatment for disintegration of cephalosporin mycelial dreg (CMD) and degradation of residual cephalosporin antibiotics, J. Hazard. Mater. 331 (2017) 265–272.

[8] Y. Zhao, X. Liang, Y. Wang, H. Shi, E. Liu, J. Fan, X. Hu, Degradation and removal of Ceftriaxone sodium in aquatic environment with Bi2WO6/g-C3N4 photocatalyst, J. Colloid Interface Sci. 523 (2018) 7–17.

[9] P. Karungamye, A. Rugaika, K. Mtei, R. Machunda, A review of methods for removal of ceftriaxone from wastewater, J. Xenobiotics 12 (3) (2022) 223–235.

[10] E. Reynoso, M.B. Spesia, N.A. García, M.A. Biasutti, S. Criado, Riboflavin-sensitized photooxidation of ceftriaxone and cefotaxime. kinetic study and effect on staphylococcus aureus, J. Photochem. Photobiol. B Biol. 142 (2015) 35–42.

[11] S.Y. Hashemi, M. Yegane Badi, H. Pasalari, A. Azari, H. Arfaeinia, A. Kiani, Degradation of Ceftriaxone from aquatic solution using a heterogeneous and reusable O3/UV/Fe3O4@ TiO2 systems: operational factors, kinetics and mineralisation, Int. J. Environ. Anal. Chem. 102 (18) (2022) 6904–6920.

[12] M. Shokri, G. Isapour, S. Shamsvand, B. Kavousi, Photocatalytic degradation of ceftriaxone in aqueous solutions by immobilized TiO2 and ZnO nanoparticles: investigating operational parameters, J. Mater. Environ. Sci 7 (2016) 2843–2851.

[13] B. Tutunaru, A. Samide, S. Iordache, C. Tigae, A. Simionescu, A. Popescu, Ceftriaxone degradation in the presence of sodium halides investigated by electrochemical methods assisted by UV-Vis spectrophotometry, Appl. Sci. 11 (4) (2021) 1376.

[14] A. Takdastan, H. Sadeghi, S. Dobaradaran, L. Ma, A. Sorooshian, M. Ravanbakhsh, M. Hazrati Niari, Synthesis and characterization of γ-Fe 2 O 3 encapsulated NaY zeolites as solid adsorbent for degradation of ceftriaxone through heterogeneous catalytic advanced oxidation processes, J. Iran. Chem. Soc. 17 (2020) 725–734.

[15] G. Di Capua, N. Femia, M. Migliaro, O. Sacco, D. Sannino, K. Stoyka, V. Vaiano, Intensification of a flat-plate photocatalytic reactor performances by innovative visible light modulation techniques: A proof of concept, Chem. Eng. Process. 118 (2017) 117–123.

[16] D. Sannino, V. Vaiano, O. Sacco, N. Morante, L. De Guglielmo, G. Di Capua, N. Femia, Visible light driven degradation of terephthalic acid: optimization of energy demand by light modulation techniques, J. Photocatal. 2 (2021) 49–61.

[17] V. Vaiano, O. Sacco, G. Di Capua, N. Femia, D. Sannino, Use of visible light modulation techniques in urea photocatalytic degradation, Water 11 (8) (2019) 1642.

[18] D. Sannino, N. Morante, O. Sacco, A. Mancuso, L. De Guglielmo, G. Di Capua, N. Femia, V. Vaiano, Visible light-driven degradation of Acid Orange 7 by light modulation techniques, Photochem. Photobiol. Sci. 22 (1) (2023) 185–193.

[19] G.O. Isopencu, A. Mocanu, I.-M. Deleanu, A brief review of photocatalytic reactors used for persistent pesticides degradation, ChemEngineering 6 (6) (2022) 89.

[20] J.G. Sczechowski, C.A. Koval, R.D. Noble, Evidence of critical illumination and dark recovery times for increasing the photoefficiency of aqueous heterogeneous photocatalysis, J. Photochem. Photobiol. A Chem. 74 (2–3) (1993) 273–278.

[21] A. Mancuso, O. Sacco, D. Sannino, S. Pragliola, V. Vaiano, Enhanced visible-light-driven photodegradation of Acid Orange 7 azo dye in aqueous solution using Fe-N co-doped TiO2, Arab. J. Chem. 13 (11) (2020) 8347–8360.

[22] A. Mancuso, O. Sacco, V. Vaiano, D. Sannino, V. Venditto, S. Pragliola, N. Morante, Visible light active Fe-N Codoped TiO2 synthesized through sol gel method: influence of operating conditions on photocatalytic performances, Chem. Eng. Trans. 86 (2021) 565–570.

[23] V. Vaiano, M. Matarangolo, O. Sacco, UV-LEDs floating-bed photoreactor for the removal of caffeine and paracetamol using ZnO supported on polystyrene pellets, Chem. Eng. J. 350 (2018) 703–713.

[24] I. Moreno, M. Avendaño-Alejo, R.I. Tzonchev, Designing light-emitting diode arrays for uniform near-field irradiance, Appl. Opt. 45 (10) (2006) 2265–2272.

[25] P. Bhattacharya, Semiconductor Optoelectronic Devices, Prentice-Hall Inc, 1997.

[26] O. Sacco, V. Vaiano, L. Rizzo, D. Sannino, Intensification of ceftriaxone degradation under UV and solar light irradiation in presence of phosphors based structured catalyst, Chem. Eng. Process.-Process Intensif. 137 (2019) 12–21.

[27] D. Sannino, V. Vaiano, P. Ciambelli, L. Isupova, Mathematical modelling of the heterogeneous photo-Fenton oxidation of acetic acid on structured catalysts, Chem. Eng. J. 224 (2013) 53–58.

[28] N. AttariKhasraghi, K. Zare, A. Mehrizad, N. Modirshahla, M.A. Behnajady, Achieving the enhanced photocatalytic degradation of ceftriaxone sodium using CdS-gC 3 N 4 nanocomposite under visible light irradiation: RSM modeling and optimization, J. Inorg. Organomet. Polym Mater. 31 (2021) 3164–3174.

[29] A.I. Cnr, Metodo 8060 di valutazione della tossicità acuta con Artemia sp, Manuali e Linee Guida-Metodi Analitici per Le Acque 3 (2003) 1043–1049.

[30] L. Albarano, S. Serafini, M. Toscanesi, M. Trifuoggi, V. Zupo, M. Costantini, D. A. Vignati, M. Guida, G. Libralato, Genotoxicity set up in artemia franciscana nauplii and adults exposed to phenanthrene, naphthalene, fluoranthene, and benzo (k) fluoranthene, Water 14 (10) (2022) 1594.

[31] M.W. Pfaffl, A new mathematical model for relative quantification in real-time RT–PCR, Nucleic Acids Res. 29 (9) (2001) e45–e.

[32] M.W. Pfaffl, G.W. Horgan, L. Dempfle, Relative expression software tool (REST©) for group-wise comparison and statistical analysis of relative expression results in real-time PCR, Nucleic Acids Res. 30 (9) (2002) e36–e.

[33] M.C. Biesinger, Accessing the robustness of adventitious carbon for charge referencing (correction) purposes in XPS analysis: insights from a multi-user facility data review, Appl. Surf. Sci. 597 (2022) 153681.

[34] B. Bonelli, O. Tammaro, F. Martinovic, R. Nasi, G. Dell'Agli, P. Rivolo, F. Giorgis, N. Ditaranto, F.A. Deorsola, S. Esposito, Reverse micelle strategy for the synthesis

of MnO x–TiO2 active catalysts for NH3-selective catalytic reduction of NO x at both low temperature and low Mn content, ACS Omega 6 (38) (2021) 24562–24574.

[35] N.C. Saha, H.G. Tompkins, Titanium nitride oxidation chemistry: An x-ray photoelectron spectroscopy study, J. Appl. Phys. 72 (7) (1992) 3072–3079.

[36] J. Du, G. Zhao, Y. Shi, Y. Li, G. Zhu, Y. Mao, R. Sa, W. Wang, A facile method for synthesis of N-doped TiO2 nanooctahedra, nanoparticles, and nanospheres and enhanced photocatalytic activity, Appl. Surf. Sci. 273 (2013) 278–286.

[37] A. Mancuso, N. Morante, M. De Carluccio, O. Sacco, L. Rizzo, M. Fontana, S. Esposito, V. Vaiano, D. Sannino, Solar driven photocatalysis using iron and chromium doped TiO2 coupled to moving bed biofilm process for olive mill wastewater treatment, Chem. Eng. J. 450 (2022) 138107.

[38] S.A. Ansari, M.H. Cho, Highly visible light responsive, narrow band gap TiO2 nanoparticles modified by elemental red phosphorus for photocatalysis and photoelectrochemical applications, Sci. Rep. 6 (1) (2016) 25405.

[39] J. Liqiang, Q. Yichun, W. Baiqi, L. Shudan, J. Baojiang, Y. Libin, F. Wei, F. Honggang, S. Jiazhong, Review of photoluminescence performance of nano-sized semiconductor materials and its relationships with photocatalytic activity, Sol. Energy Mater. Sol. Cells 90 (12) (2006) 1773–1787.

[40] K. Selvam, S. Balachandran, R. Velmurugan, M. Swaminathan, Mesoporous nitrogen doped nano titania—A green photocatalyst for the effective reductive cleavage of azoxybenzenes to amines or 2-phenyl indazoles in methanol, Appl. Catal. A 413 (2012) 213–222.

[41] E. Wang, T. He, L. Zhao, Y. Chen, Y. Cao, Improved visible light photocatalytic activity of titania doped with tin and nitrogen, J. Mater. Chem. 21 (1) (2011) 144–150.

[42] D. Li, H. Haneda, S. Hishita, N. Ohashi, Visible-light-driven N− F− codoped TiO2 photocatalysts. 2. Optical characterization, photocatalysis, and potential application to air purification, Chem. Mater. 17 (10) (2005) 2596–2602.

[43] Y. Cong, J. Zhang, F. Chen, M. Anpo, Synthesis and characterization of nitrogen-doped TiO2 nanophotocatalyst with high visible light activity, J. Phys. Chem. C 111 (19) (2007) 6976–6982.

[44] T. Ohsaka, F. Izumi, Y. Fujiki, Raman spectrum of anatase, TiO2, J. Raman Spectrosc. 7 (6) (1978) 321–324.

[45] R. Vinodh, A. Abidov, M.M. Peng, C.M. Babu, M. Palanichamy, W.S. Cha, H.-T. Jang, A new strategy to synthesize hypercross-linked conjugated polystyrene and its application towards CO 2 sorption, Fibers Polym. 16 (2015) 1458–1467.

[46] J.-M. Herrmann, Heterogeneous photocatalysis: state of the art and present applications In honor of Pr. RL Burwell Jr.(1912–2003), Former Head of Ipatieff Laboratories, Northwestern University, Evanston (Ill), Topics in catalysis 34 (2005) 49-65.

[47] M. Náfrádi, T. Alapi, G. Bencsik, C. Janáky, Impact of reaction parameters and water matrices on the removal of organic pollutants by TiO2/LED and ZnO/LED heterogeneous photocatalysis using 365 and 398 nm radiation, Nanomaterials 12 (1) (2021) 5.

[48] N. Rioja, S. Zorita, F.J. Peñas, Effect of water matrix on photocatalytic degradation and general kinetic modeling, Appl Catal B 180 (2016) 330–335.

[49] A.R.L. Ribeiro, N.F. Moreira, G.L. Puma, A.M. Silva, Impact of water matrix on the removal of micropollutants by advanced oxidation technologies, Chem. Eng. J. 363 (2019) 155–173.

[50] X. Cheng, L. Liang, J. Ye, N. Li, B. Yan, G. Chen, Influence and mechanism of water matrices on H2O2-based Fenton-like oxidation processes: a review, Sci. Total Environ. (2023), 164086.

[51] J.R. Bolton, K.G. Bircher, W. Tumas, C.A. Tolman, Figures-of-merit for the technical development and application of advanced oxidation technologies for both electric-and solar-driven systems (IUPAC Technical Report), Pure Appl. Chem. 73 (4) (2001) 627–637.

[52] N. Apostolescu, R.E. Tataru Farmus, M. Harja, M.A. Vizitiu, C. Cernatescu, C. Cobzaru, G.A. Apostolescu, Photocatalytic removal of antibiotics from wastewater using the CeO2/ZnO heterojunction, Materials 16 (2) (2023) 850.

[53] K. Baruah, P. Norouzitallab, R.J. Roberts, P. Sorgeloos, P. Bossier, A novel heat-shock protein inducer triggers heat shock protein 70 production and protects Artemia franciscana nauplii against abiotic stressors, Aquaculture 334 (2012) 152–158.

[54] K. Baruah, J. Ranjan, P. Sorgeloos, P. Bossier, Efficacy of heterologous and homologous heat shock protein 70s as protective agents to Artemia franciscana challenged with Vibrio campbellii, Fish Shellfish Immunol. 29 (5) (2010) 733–739.

[55] I. Varó, A. Perini, A. Torreblanca, Y. Garcia, E. Bergami, M.L. Vannuccini, I. Corsi, Time-dependent effects of polystyrene nanoparticles in brine shrimp Artemia franciscana at physiological, biochemical and molecular levels, Sci. Total Environ. 675 (2019) 570–580.

[56] Y. Chen, S. Zhou, H. Yang, L. Wu, Structure and properties of polyurethane/nanosilica composites, J. Appl. Polym. Sci. 95 (5) (2005) 1032–1039.

[57] J. Han, Y. Park, H.H. Shin, A.-Y. Shin, H.-M. Kang, J. Lee, Y.-U. Choi, K.-W. Lee, Effects of dinoflagellate Gymnodinium catenatum on swimming behavior and expression of heat shock protein (hsp) genes in the brine shrimp Artemia franciscana, Harmful Algae 110 (2021) 102146.